Journal of Thermal Analysis and Calorimetry (2022) 147:13375–13387
https://doi.org/10.1007/s10973-022-11670-4

Thermal, optical and temperature-dependent electrical properties of poly(aniline-*co*-pyrrole)/copper alumina nanocomposites for optoelectronic devices

S. Sankar[1] · **M. T. Ramesan**[1]

Received: 18 March 2022 / Accepted: 26 September 2022 / Published online: 10 October 2022

Abstract

The article deals with the investigation of structural, thermal and temperature-dependent alternating current (AC) parameters of hetero-structures generated by the reinforcement of copper alumina (Cu–Al_2O_3) nanoparticles within the poly(aniline-*co*-pyrrole) (PANI-*co*-PPy). Further, the effect of reinforcement of Cu–Al_2O_3 on the direct current (DC) conductivity of the copolymer was equated with various theoretical models. Compared with the pristine copolymer, the ultraviolet–visible (UV–visible) spectrum of (PANI-*co*-PPy)/Cu–Al_2O_3 nanocomposites manifested a redshift in absorbance and the least optical bandgap energy was observed for 5 mass percentage (mass %) nanocomposite. Field emission scanning electron microscopy confirmed the effective reinforcement of Cu–Al_2O_3 nanoparticles within the PANI-*co*-PPy. The thermogravimetric analysis profile demonstrated a delayed thermal degradation for copolymer nanocomposites. The alternating current (AC) conductivity and dielectric properties were enhanced with a rise in temperature and content of nanofillers (up to 5 mass % loading). Further, the activation energy was found to be reduced with the temperature indicating the semiconductive behavior of synthesized nanocomposites. The Nyquist plot of copolymer nanocomposites showed two distinct areas, an incomplete semicircle and a rapid spike. The diameter of the semicircle was decreased with temperature. The DC conductivity of nanocomposites was enhanced with the reinforcement of Cu–Al_2O_3 nanofillers due to the enriched number of charge carriers accumulated within the nanocomposites. Finally, DC conductivity values were equated using Scarisbrick, Bueche and McCullough theoretical models. The McCullough model was in good agreement with measured DC conductivity as this model explains the dependence of DC conductivity with the quantity of filler and conductive pathway generated between the interfaces. Based on the results, these synthesized copolymer composites can be used in highly durable electronic devices such as supercapacitors, electrochemical sensors and optoelectronics.

Keywords Poly(aniline-*co*-pyrrole) · Copper alumina · Nanocomposites · Optical properties · Thermal stability · Temperature-dependent conductivity · Dielectric parameters · DC conductivity modeling

Introduction

Conducting polymers pertain to the class of organic semiconductors with alluring material properties [1, 2]. The fascinating electrical properties, optical traits and stability could be adopted for fabricating high-tech devices. The quasi-1D internment to electron transfer plays a significant role in controlling the electronic properties of conducting polymer. On account of superior electrical traits and environmental stability, polyaniline (PANI) and polypyrrole (PPy) are extensively accepted as smart conducting polymers [3–6]. However, the poor processability and solubility are the major flaws of the aforementioned conducting polymers. In recent years, scientists have been trying to solve the aforementioned flaws experienced by conducting polymers through copolymerization methods [7, 8]. Simultaneously, PANI-*co*-PPy owns exclusive electrochemical properties than polyaniline and polypyrrole.

Copolymers with TiO_2 and Fe_3O_4 nanocomposites can incorporate physical and chemical traits of two individual polymers with electrical and magnetic traits of metallic

---

M. T. Ramesan
mtramesan@uoc.ac.in

[1] Department of Chemistry, Centre for Polymer Science and Technology, University of Calicut, Calicut University P.O., Malappuram, Kerala 673 635, India

nanoparticles [9, 10]. The aforementioned hybrid materials generally express a batch of physicochemical properties remarkably unique from the isolated constituents. The properties of the hybrid could be well utilized in ingenious multifunctional devices. The amplification of properties is dependent on the quantity of nanofillers used in the composite. The synergy between organic macromolecular chains and metallic nanofillers is the reason for the aforementioned amplification in properties [11]. Among the set of metallic nanofillers, metal oxide nanoparticles are widely recognized owing to their standard electrical, optical, sensing and photocatalytic properties [12–15]. The previous reports suggested that metal oxide nanoparticles such as ZnO, TiO_2, Fe_3O_4 impart optical properties, electrical conductivity and thermal stability to conducting polymer matrix [7, 9, 16].

Alumina nanoparticles are excellent materials with impressive thermomechanical and optical properties [17–19]. On the other side, moderate electrical properties thwart their usage in electrical applications. Previous reports suggested that dispersive strengthening of alumina with copper has a significant impact on improving their electrical properties [20]. Earlier, our research group has been successful in synthesizing nanocomposites of PANI with Cu–Al_2O_3 having favorable thermal and electrical properties [21]. This incites us to use Cu–Al_2O_3 nanomaterials as filler particles to reinforce the PANI-*co*-PPy matrix.

Electro-polymerization, in situ chemical oxidation polymerization, melt mixing, solution mixing and mechanical mixing are outstanding polymerization modes implemented for the preparation of conducting polymer nanocomposites [22–25]. By the means of electro-polymerization technique, we can fabricate conducting polymer nanocomposite films while the lower yield of polymerization and convoluted experimental setup are the concerns. In situ oxidation polymerization is a benign technique to get conducting polymer nanocomposites in powder form with a higher yield. In situ chemical oxidation polymerization of almost all conducting polymers is performed in aqueous condition hence can be considered a green synthetic procedure. Through the in situ polymerization technique, uniform coverage of nanofillers over conducting polymers establishes a synergy between the constituents and eventually experiences magnificent material properties [26]. The purpose of this article was to synthesize and investigate the optical, morphological, temperature-dependent dielectric properties and DC conductivity studies of (PANI-*co*-PPy)/Cu–Al_2O_3 nanocomposites. The change in DC conductivity of the copolymer with the addition of Cu–Al_2O_3 nanoparticles was also correlated with different theoretical modeling to establish the mechanism of conductivity in the copolymer nanocomposites.

Experimental

Materials and methods

The aniline and pyrrole were acquired from Merck and were distilled prior to use. The oxidant ($FeCl_3$), surfactant (sodium dodecyl sulfate (SDS)) HCl and methanol were purchased from Hi-media. The materials for the synthesis of copper alumina nanofillers (Cu $(NO_3)_2$, Al $(NO_3)_3$ and urea) were also bought from Merck. Distilled water was used for the entire course of synthesis. The Cu–Al_2O_3 nanopowder with a particle size of 30 nm was prepared through the sol–gel auto-combustion technique [21]

Synthesis of poly(aniline-*co*-pyrrole)

The polymerization of monomer solutions containing an equal concentration of aniline and pyrrolewas achieved by chemical oxidation polymerization. The oxidizing agent was taken in a three-neck flask by dissolving an appropriate quantity of $FeCl_3$ in water at 0 °C. The acidic aqueous monomer solutions were added drop by drop using a dropping funnel into the $FeCl_3$ solution. The color change of the polymeric solution manifests the polymerization reaction. The efficient polymerization was ensured by constant stirring and keeping the reaction mixture at 0 °C for 8 h. Then, impurities such as excess monomers and oxidants left were washed with water and methanol. The copolymer was kept in a vacuum oven maintained at 60 °C for 24 h.

Synthesis of (PANI-*co*-PPy)/Cu–Al_2O_3 nanocomposites

The encapsulation of Cu–Al_2O_3 within the PANI-*co*-PPy matrix was achieved by following the aforementioned reaction strategy in the presence of different contents of copper alumina nanoparticles (3, 5 and 7 mass %).

Instrumentation

The UV spectrum of PANI-*co*-PPy and their nanocomposites with Cu–Al_2O_3 were recorded using a JASCO V-770 spectrophotometer. The field emission scanning electron microscopy (FE-SEM) images of (PANI-*co*-PPy)/Cu–Al_2O_3 nanocomposite were studied using the Carl Zeiss VP-500 model. Evaluation of the thermal stability of (PANI-*co*-PPy)/Cu–Al_2O_3 in the temperature range of 25–600 °C at a heating rate of 10 °C min^{-1} was performed on Hitachi STA7200 thermogravimetric analyzer. The frequency-dependent AC conductivity, dielectric permittivity and impedance parameters of pelletized samples (0.5 mm thickness and 1.5 cm diameter) at different

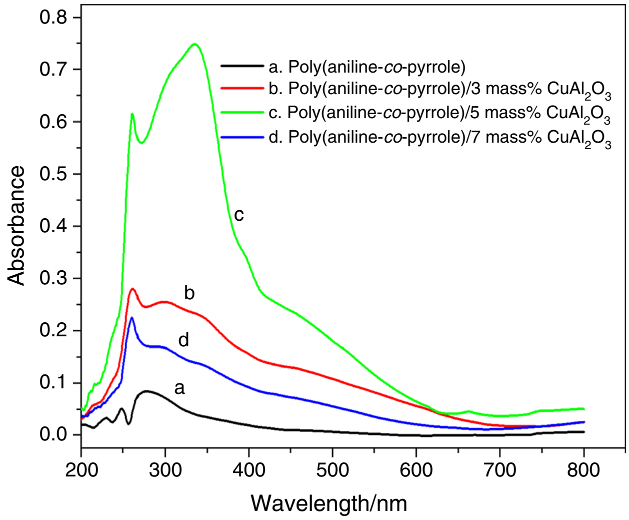

Fig. 1 UV- visible spectrum of poly(aniline-*co*-pyrrole) and its nanocomposites

temperatures were measured with the help of the Hioki 3570 Model.

Results and discussion

UV–visible spectroscopy

The UV–visible spectrum of (PANI-*co*-PPy)/Cu–Al_2O_3 nanocomposites at different loadings is presented in Fig. 1. The absorption spectrum of all samples shows a single absorption at 274 nm. This absorption band arises from the electron transition from a filled π orbital (HOMO) to π^* orbital (LUMO). The absorption of a copolymer greatly depends on the degree of ordering of the chains in the polymeric material. The noticeable red shift in absorption band and increased relative intensity of absorption are evident with the loading of Cu–Al_2O_3 nanofiller in the copolymer. This arises from the excellent order of (PANI-*co*-PPy)/Cu–Al_2O_3 nanocomposites and increased defect sites. The maximum absorption intensity of (PANI-*co*-PPy)/5 mass % nanocomposite implies regular and consistent dispersion of Cu–Al_2O_3. This means that the interaction between nanofiller and copolymer is maximum at this loading. The reduction in absorption maximum in the 7 mass % copolymer nanocomposite indicates a reduction in interfacial interaction due to the clustering of nanofillers.

Optical bandgap energy

The optical bandgap decides whether a material is suitable for optoelectronic applications or not. Bandgap energy signifies the energy separation existing between the valence band and conduction band. By the Tauc equation, we will be able to measure the direct optical bandgap energy.

$$(\propto h\gamma)^2 = B(h\gamma - Eg) \tag{1}$$

(α) in the equation corresponds to absorption coefficient, B is the probability transition constant, $h\nu$ is the excitation energy and Eg refers to optical bandgap energy. The absorption coefficient can be calculated by the equation given below.

$$\alpha = \frac{\text{Absorbance}}{\text{Path length}} \tag{2}$$

The Tauc plot of PANI-*co*-PPy and (PANI-*co*-PPy)/Cu–Al_2O_3 nanocomposites is shown in Fig. 2. It is observed that the bandgap energy of PANI-*co*-PPy reduces with the incorporation of nanofillers. This observation is the result of an intermediary energy level originated between the conduction band and valence band. With the help of an intermediate band, facile electron excitation is possible. Moreover, the generation of charge carriers in the copolymer associated with the incorporation of Cu–Al_2O_3 fillers widens the density of states in the direction of the visible region. The (PANI-*co*-PPy)/5 mass % Cu–Al_2O_3 shows the least value for bandgap energy which confirms the presence of a large number of charge carriers within the system. The consistent distribution of fillers and the efficient interaction between copolymer and Cu–Al_2O_3 is the reason for an increased number of charge carriers. The countless intermediate energy levels generated in the aforementioned system reduce the optical bandgap energy. The increase in bandgap energy beyond 5 mass % loading of nanofiller is due to the clustering tendency of nanoparticles in the copolymer matrix.

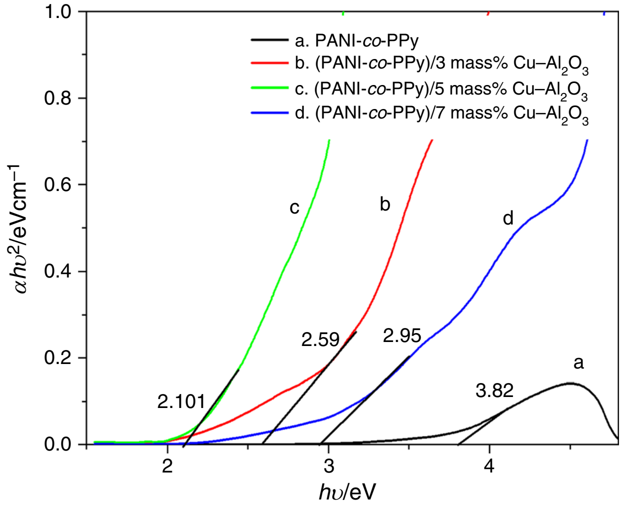

Fig. 2 Optical bandgap studies of poly(aniline-*co*-pyrrole) and its nanocomposites

Field emission scanning electron microscopy (FE-SEM)

FE-SEM images of PANI-*co*-PPy and (PANI-*co*-PPy)/Cu–Al_2O_3 nanocomposites are analyzed, and the images are given in Fig. 3. The FE-SEM photograph of (PANI-*co*-PPy) is observed to have a corrugated morphology. Thus, constant morphology throughout the surface with consistent particle sizes confirms the copolymerization reaction occurs between aniline and pyrrole. However, a spherical morphology is obtained for (PANI-*co*-PPy)/Cu–Al_2O_3 nanocomposites. This morphology arises from the interaction between Cu–Al_2O_3 and PANI-*co*-PPy. Further, with the addition of Cu–Al_2O_3 nanoparticles to PANI-*co*-PPy, inflation in the particle size is also identified. This inflation in particle size generates a larger surface area, which is vital for superior material properties. Better morphology has been observed for 5 mass % nanocomposite with an average grain size of 82.08 nm. The lumping of particles has been observed for higher mass fraction nanocomposites which advocate the co-mixing of Cu–Al_2O_3 nanomaterials in the PANI-*co*-PPy abutment. The co-mixing of Cu–Al_2O_3 nanomaterials debilitates the interaction at the interface between copolymer and nanoparticles.

TG analysis

With the aid of TG analysis, we can identify the effect of Cu–Al_2O_3 nanoparticles on the thermal stability of PANI-*co*-PPy. Figure 4 depicts the TG graph of PANI-*co*-PPy and (PANI-*co*-PPy)/Cu–Al_2O_3. Two recognizable mass loss has observed for bare PANI-*co*-PPy. The first mass loss between room temperature and 146 °C corresponds to the expulsion of water molecules and decomposition of dopant ions, respectively. The second and final mass loss corresponds to the gradual degradation of the copolymer matrix. The ultimate char residue found at 600 °C for bare PANI-*co*-PPy is 55 mass %. The polymer degradation temperature and ultimate char residue (at 600 °C) of copolymer nanocomposites are found to be greater than that of the pristine copolymer. The thermal stability and ultimate char residue of (PANI-*co*-PPy)/Cu–Al_2O_3 nanocomposites are maximum for higher mass fractions. The thermal resistance of Cu–Al_2O_3 nanoparticles and their strong interaction with the polymer matrix

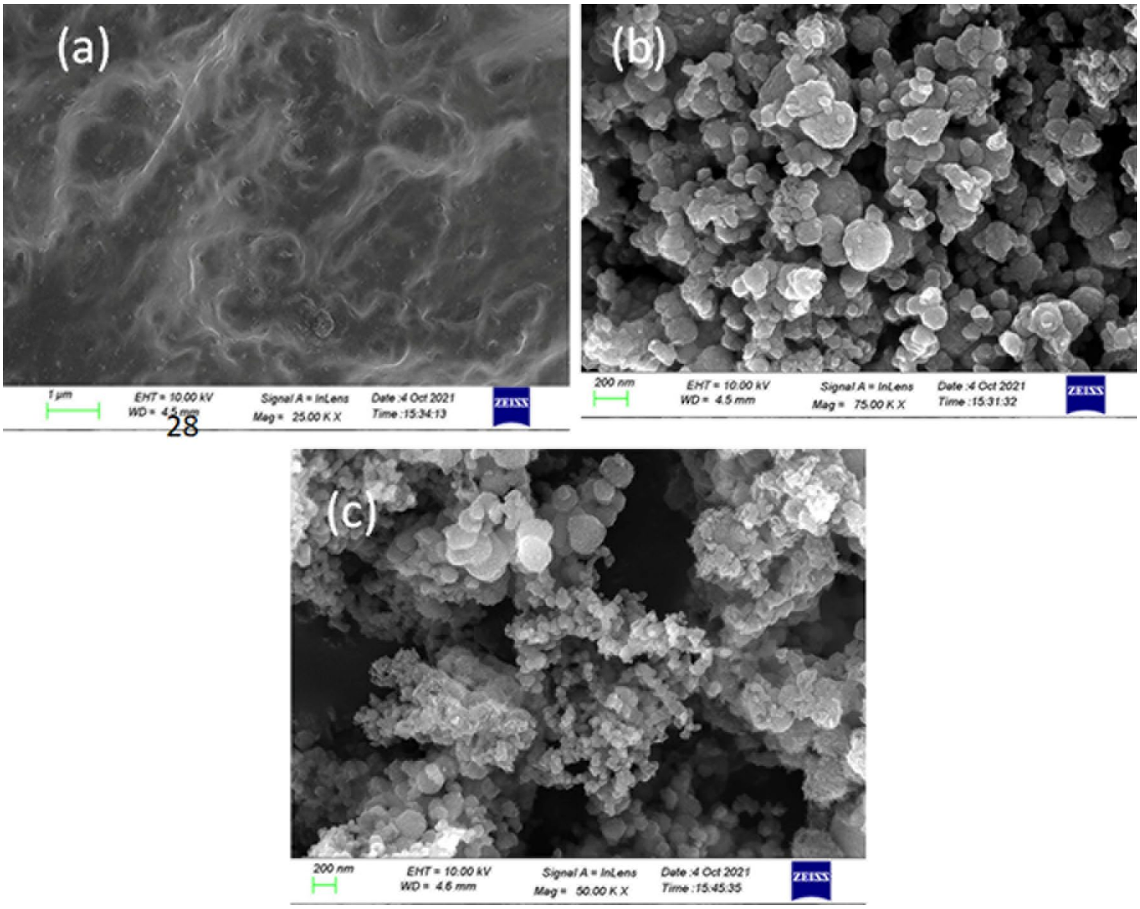

Fig. 3 FE-SEM images of **a** copolymer **b** 5 mass % and **c** 7 mass % of Cu–Al_2O_3

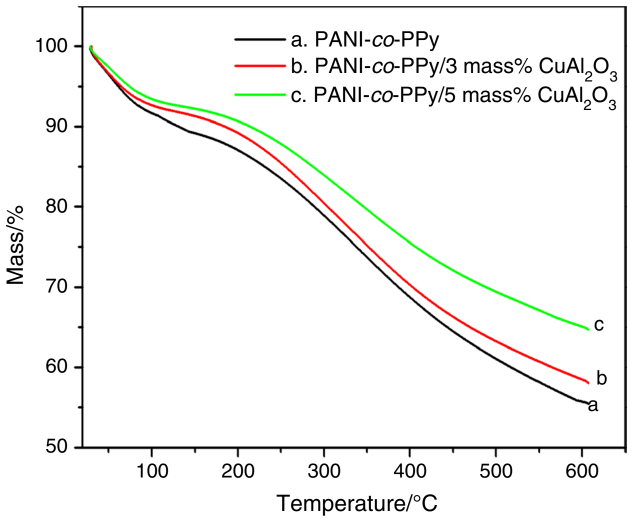

Fig. 4 TG pattern of poly(aniline-*co*-pyrrole) and Cu–Al$_2$O$_3$ nanocomposites

can be attributed to the thermal stability and flame resistance of (PANI-*co*-PPy)/Cu–Al$_2$O$_3$ nanocomposites [27].

Dielectric constant

The details and statistics regarding the polarization behavior of PANI-*co*-PPy and their nanocomposite with Cu–Al$_2$O$_3$ fillers can be obtained by measuring the dielectric parameters over a series of frequencies at various temperatures. Figure 5 denotes the variation of the dielectric constant of PANI-*co*-PPy and (PANI-*co*-PPy)/Cu–Al$_2$O$_3$ nanocomposite (3, 5 and 7 mass % loading) with frequency at different temperatures. For the entire set of samples, higher values for dielectric constant are noticed at 100 Hz. The Maxwell–Wagner–Sillars and counter ion polarization effects can be ascribed to the high dielectric values [28]. Once the frequency is increased, the dielectric constant decreases due to the rapid switching of polarity of the AC electric field. This expeditious reversibility of polarity restricts the polarization within the conducting copolymer. Further, it is observed that the dielectric constant of all samples improves with the temperature rise. At room temperature, the dipoles within the

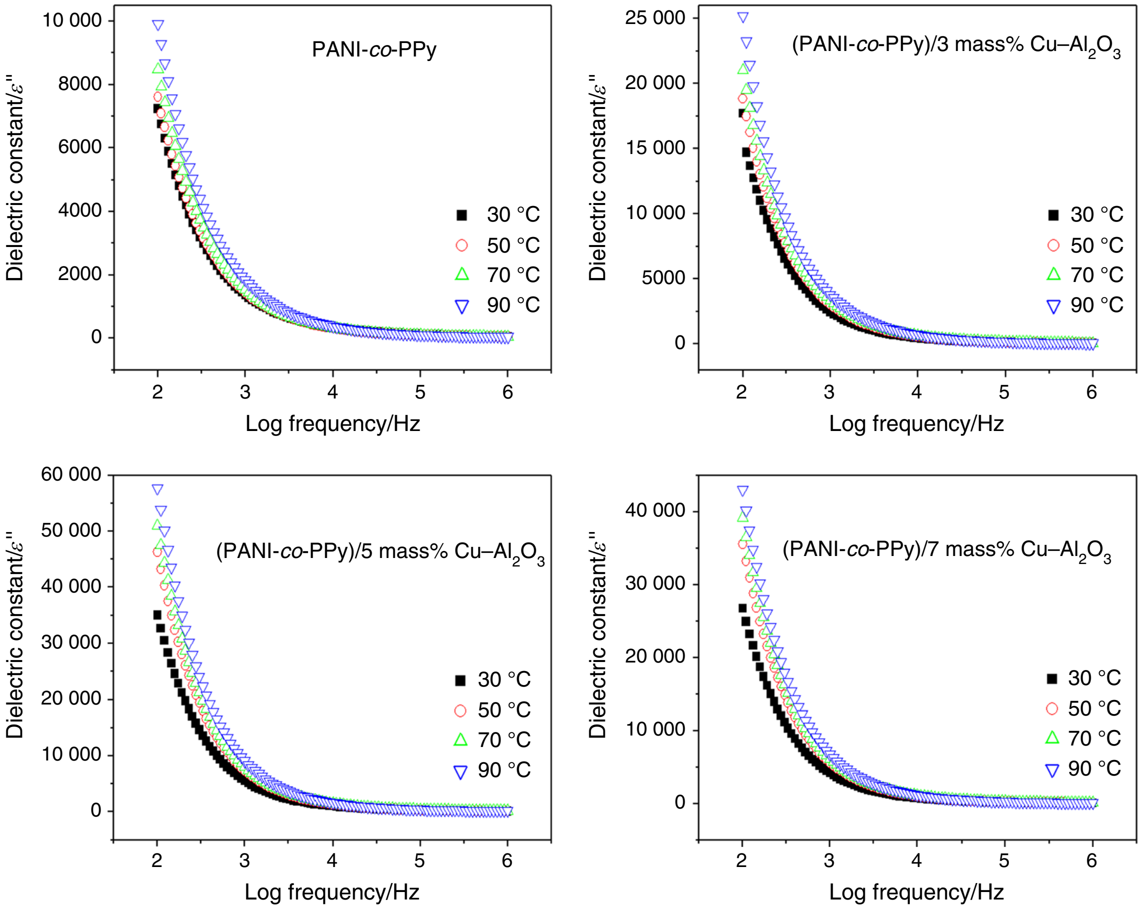

Fig. 5 Variation of dielectric constant of poly(aniline-*co*-pyrrole) its nanocomposites

material cannot align with the field thereby minimizing the Maxwell–Wagner–Sillars polarization effect. On the other hand, increasing the temperature aids the aligning of dipoles with the field eventually maximizing the polarization and enhancing the dielectric constant values [29].

Figure 6 denotes the dielectric constant V_s fraction of Cu–Al_2O_3 nanofillers reinforced at 90 °C at a frequency of 100 Hz. It is obvious that values of dielectric constant improve with the incorporation of Cu–Al_2O_3 nanofillers. The maximum value of the dielectric constant is observed for (PANI-*co*-PPy)/5 mass % Cu–Al_2O_3 nanocomposite, and this can be attributed to the excellent electron tunneling between the interface facilitated by the homogenous distribution of Cu–Al_2O_3 nanofillers (already discussed in SEM results). However, the loading of nanoparticles reached 7 mass %, and the dielectric constant is found to diminish due to the self-bounding of nanofillers within the copolymer which restricts the charge tunneling between the interface [30].

Dielectric loss tangent

The plot of Tan δ with frequency shown in Fig. 7 gives us information about energy dissipation occurring in (PANI-*co*-PPy)/Cu–Al_2O_3 nanocomposites (0, 3, 5 and 7 mass % loading) when exposed to an electric field at different temperatures. It is observed that the magnitude of Tan δ is reduced on increasing the frequency. The highest energy dissipation at lower frequencies is due to the presence of insulating grain boundaries. At higher frequencies, the energy dissipation is almost saturated due to lower polarization occurring in the system [31]. The energy dissipation of the studied material is greatly influenced by temperature. The rapid oscillation of charges induced by temperature is the reason for the aforementioned observation. Additionally, the energy dissipation is increased by the introduction of Cu–Al_2O_3 within the PANI-*co*-PPy system. The increased hopping of charge carriers in nanocomposites is the reason for the highest energy dissipation. The maximum energy dissipation is observed for (PANI-*co*-PPy)/5 mass % Cu–Al_2O_3 nanocomposite. The excellent structural regularity in this composite facilitates the large-scale hopping of charge carriers. The aggregation tendency of Cu–Al_2O_3 nanofillers in (PANI-*co*-PPy)/7 mass % restricts hopping of charges, and hence, a reduction in energy dissipation is observed.

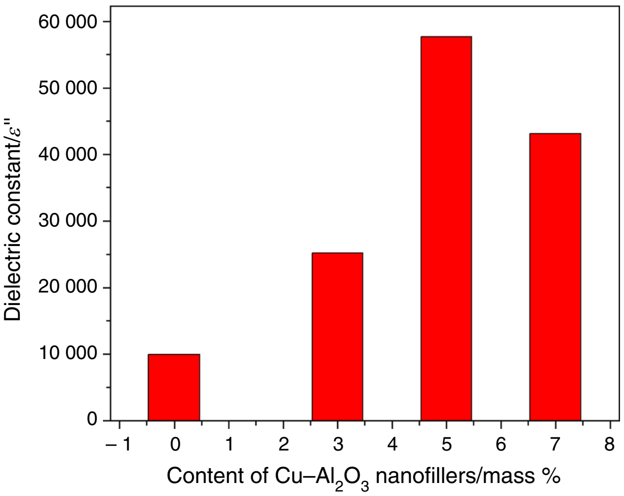

Fig. 6 Variation of dielectric constant copolymer nanocomposites at higher temperature

Alternating current conductivity (AC)

The AC conductivity V_s frequency plot of (PANI-*co*-PPy) and its nanocomposites at different temperatures (30, 50, 70 and 90 °C) is given in Fig. 8. The AC conductivity value of bare copolymer is found to be unvarying at lower frequency ranges. This frequency independence arises from the DC conductance where unbounded or loosely bounded charges are active. While these charges are inadequate to show a notable change in conductivity values. On the other hand, up to 10^4 Hz, a slight lowering of AC conductivity values is observed for (PANI-*co*-PPy)/Cu–Al_2O_3 nanocomposites. This anomalous behavior at lower frequencies can be explained on the basis of delayed dynamics of charge carriers present in the heterogeneous system. This delayed motion of charge carriers occurs at the onset of electrode polarization. Unlike at lower frequencies, for all samples, large variations in AC conductivity values are observed at higher frequencies. Here, the conductivity arises from bound charges. A large number of bound charges within the polymeric system get activated at larger frequencies hence obeying the power law. The high temperatures enable the unbounding of charge carriers that can easily tunnel through the frequency barricade hence enhancing the conductivity. We can observe the temperature dependence of AC conductivity of the copolymer and their hybrid system from the graph. The induced thermal energy activates the charge carriers within the system hence increasing their oscillations. The thermal-induced vibration of charges results in enhanced conductivity at high temperatures [32].

The dependence of AC conductivity on filler content at 10^6 Hz and 90 °C is shown in Fig. 9. The AC conductivity values of PANI-*co*-PPy are enhanced with the addition of Cu–Al_2O_3 nanofillers. The interfacial interaction between Cu–Al_2O_3 nanofiller and copolymer reduces the inter-chain distance, creates new electrical states and eventually gives rise to new conduction paths [33]. The maximum conductivity for (PANI-*co*-PPy)/5 mass % Cu–Al_2O_3 nanocomposite arises from the efficient distribution of nanofillers. The uniform distribution of nanofillers aids the formation of

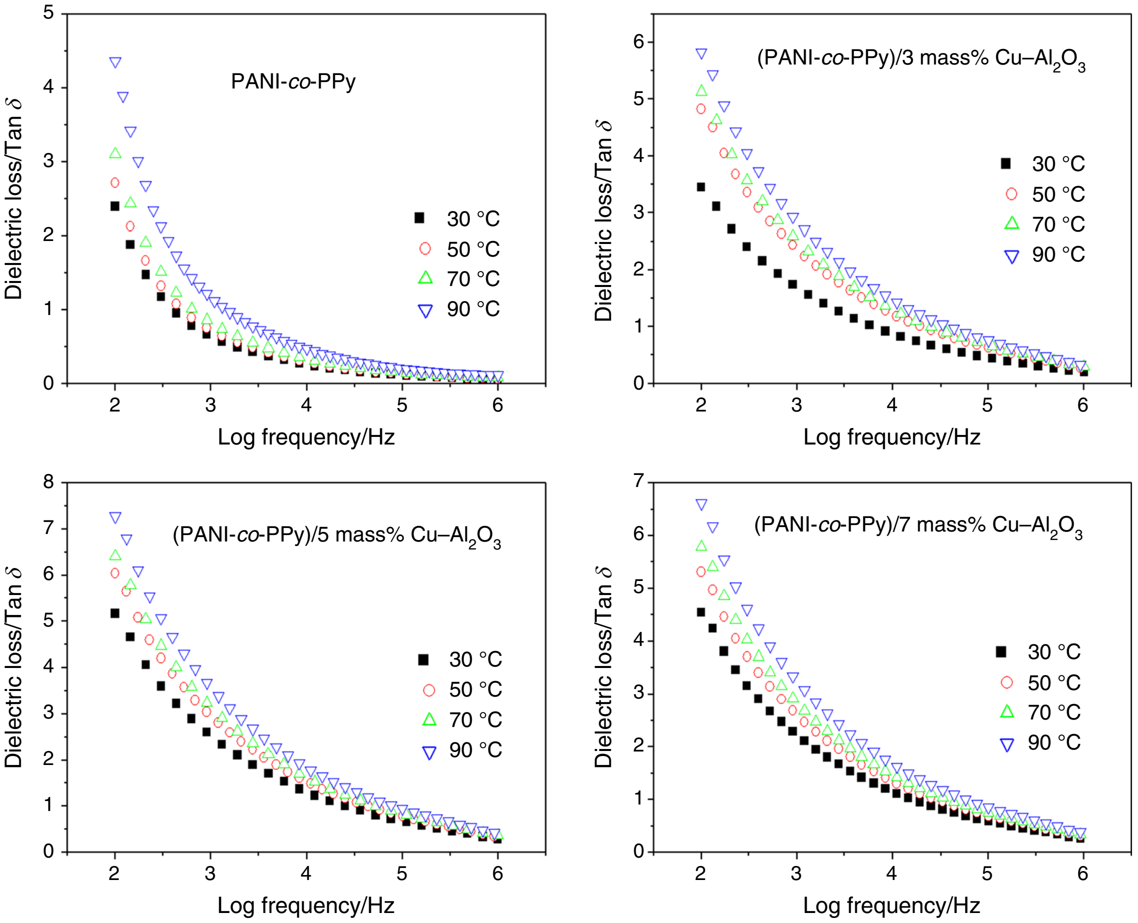

Fig. 7 Variation of dielectric loss tangent of poly(aniline-*co*-pyrrole)/Cu–Al_2O_3

interconnected conductive networks of Cu–Al_2O_3 nanofillers within the pristine PANI-*co*-PPy. The decrease in AC conductivity beyond 5 mass % Cu–Al_2O_3 nanocomposites can be attributed to the depletion of the localized sites due to the aggregation of Cu–Al_2O_3 nanofillers.

Arrhenius plot of conductivity

The temperature dependence of AC conductivity follows an Arrhenius type of relation which can be expressed as

$$\sigma_{\mathrm{ac}} = \sigma_0 \exp \frac{-E_\sigma}{KT} \tag{3}$$

where E_σ, K, T and σ_0 correspond to the activation energy, Boltzmann constant, absolute temperature and pre-exponential factor, respectively. The plot of AC conductivity V_s $1/T$ of PANI-*co*-PPy and its nanocomposites is presented in Fig. 10. The slope of this graph gives the activation energy of samples. The magnitude of activation energy V_s Cu–Al_2O_3 content at 1 MHz is shown in Fig. 11. The Cu–Al_2O_3 nanofillers reduce the conduction barrier of PANI-*co*-PPy due to the generation of charge carriers within the system. The efficient conducting pathway in (PANI-*co*-PPy)/5 mass % Cu–Al_2O_3 minimizes the energy for activation of charges and hence, shows excellent conductivity. While more energy is required for activating the charge carriers in (PANI-*co*-PPy)/7 mass % Cu–Al_2O_3 due to the aggregation of nanofillers.

Nyquist plot

Figure 12 shows the frequency dependency of the impedance of PANI-*co*-PPy and its nanocomposites at various temperatures. The real part of impedance gives insights into resistance and the imaginary part is about reactance. For all samples, both the real part and imaginary part of impedance diminish with an increase in frequencies. The rapid dipolar oscillations occurring with an increase in frequency give rise to reactive current which eventually results in the reduction in reactance and resistance. Further beyond a critical frequency, impedance becomes frequency independent. The frequency-independent impedance arises from

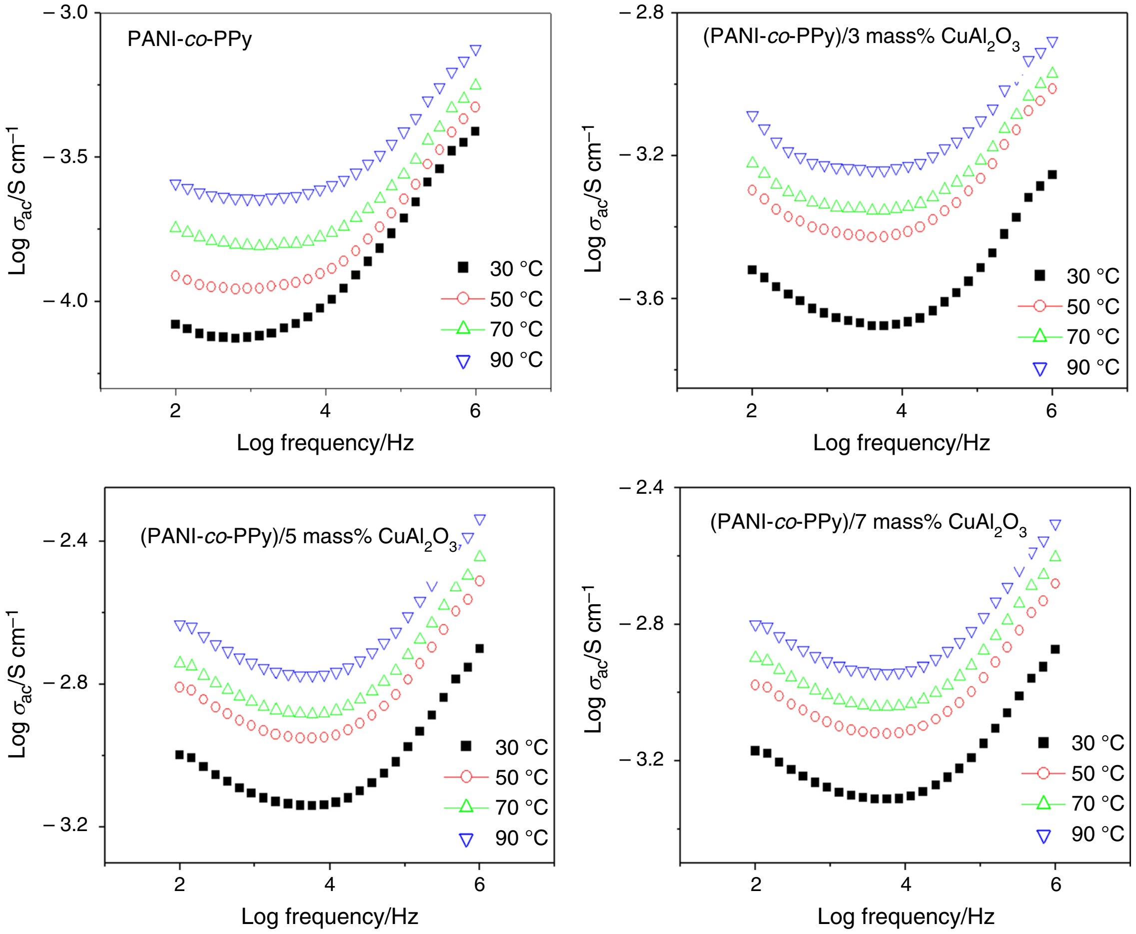

Fig. 8 The variation of AC conductivity of copolymer/Cu–Al$_2$O$_3$ at different temperatures

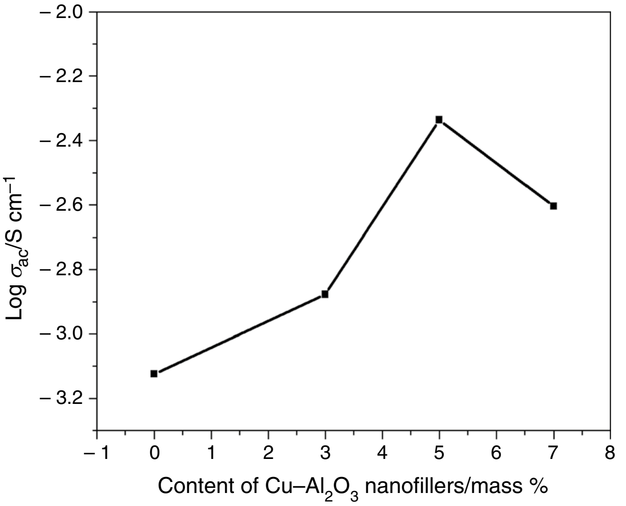

Fig. 9 The dependence of AC conductivity with various filler content at 1 MHz at 90 °C

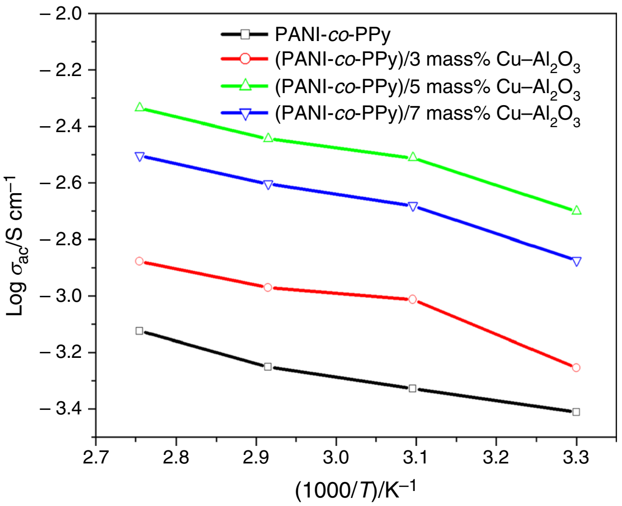

Fig. 10 The plot of AC conductivity V_s 1000/T of copolymer and its nanocomposites

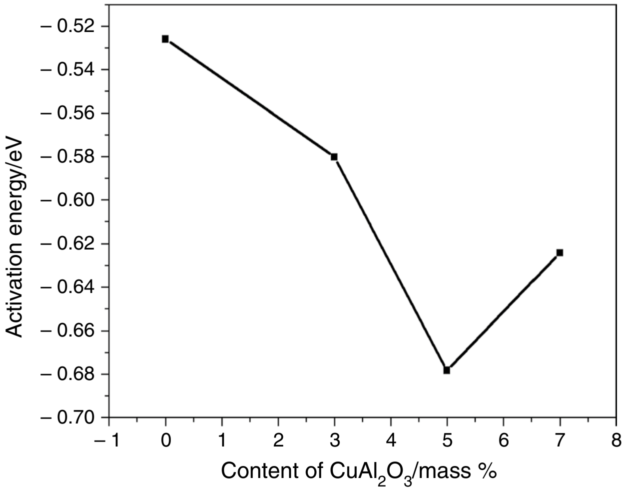

Fig. 11 The Ea V_s content of Cu–Al_2O_3 nanofillers

the insubstantial interfacial polarization at higher frequencies [34] which has already been discussed in the previous sections. With the increase in temperatures, the magnitude of Z is found to be decreasing. This observation is due to the temperature-induced mobility of charge carriers hence signifying the semiconducting nature of the samples.

With the incorporation of Cu–Al_2O_3 nanofillers, the reactance and resistance are found to decrease. Moreover, the reactance and resistance decrease with an increase in nanofiller content within the matrix. The conductive Cu–Al_2O_3 nanoparticles generate an incessant conductive framework within the hybrid systems. The generation of a conducting framework relies on homogeneity in dispersion of nanofillers. The microscopic images of (PANI-*co*-PPy)/5 mass % nanocomposite indicate the homogenous dispersion of Cu–Al_2O_3 nanofillers in the matrix and which can be correlated with their minimum values for the real and imaginary part of the impedance. Beyond 5 mass % loading, the particles have a tendency to agglomerate and this can be the reason for poor dielectric behavior of the (PANI-*co*-PPy)/7 mass % Cu–Al_2O_3 nanocomposite. The observations under this session are proving the inverse relationship of impedance with the AC conductivity section as the conductivity of all materials increases with frequency, temperature and filler loading. The Nyquist plot of (PANI-*co*-PPy)/3 mass % Cu–Al_2O_3 and (PANI-*co*-PPy)/5 mass % Cu–Al_2O_3 shown in Fig. 13

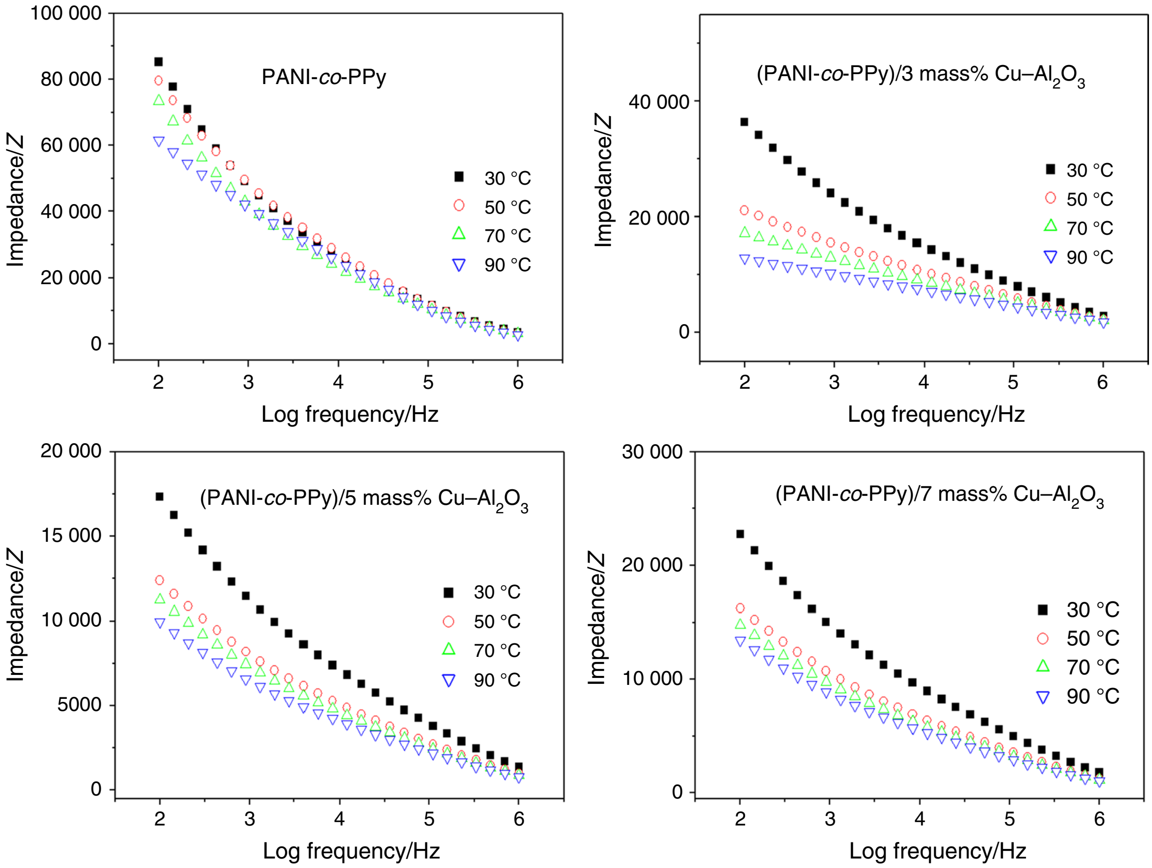

Fig. 12 The variation of impedance of copolymer/Cu–Al_2O_3 at different temperatures

Fig. 13 Nyquist plot of 3 and 5 mass % Cu–Al_2O_3 incorporated poly(aniline-*co*-pyrrole)

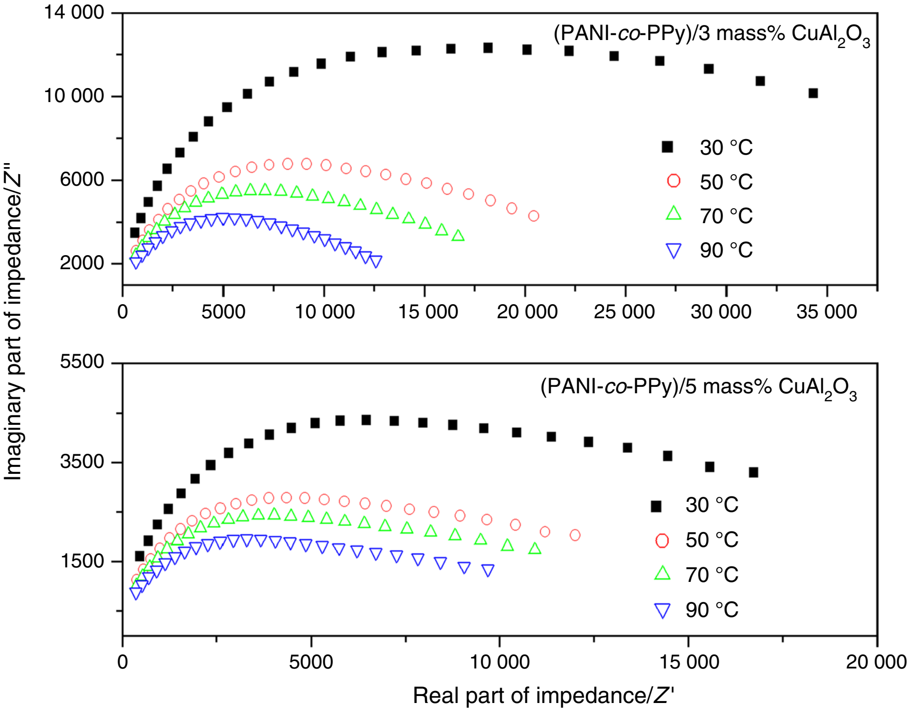

shows two distinct areas; the first one corresponding to a region of incomplete semicircles followed by a region of the sudden spike. The semi-circular region indicates the bulk resistance of the polymeric material. The sudden spike is a clear indication of double-layer capacitance in the surface connecting electrode and sample pellet. When the temperature of the sample is increased, the diameter of the semicircle decreases. This confirms the direct proportionality of AC conductivity with temperature. Additionally, the diameter of the circle is decreasing with the incorporation of Cu–Al_2O_3 nanofillers,which indicates the reduction in bulk resistance of PANI-*co*-PPy.

Direct current conductivity (DC)

DC conductivity plot of (PANI-*co*-PPy)/Cu–Al_2O_3 nanocomposites is shown in Fig. 14. An enhancement in DC conductivity of (PANI-*co*-PPy)/Cu–Al_2O_3 nanocomposites is noticed as compared to pristine PANI-*co*-PPy. The bonding association between the polar fragments of the organic and inorganic interface creates a path for charge transport. A sharp enhancement in DC conductivity of (PANI-*co*-PPy)/Cu–Al_2O_3 nanocomposites is observed with increase in the composition of nanoparticles. The enhanced crystallinity and compactness of the nanocomposites on wrapping Cu–Al_2O_3 nanofillers within the copolymer is the reason for increased conductivity.

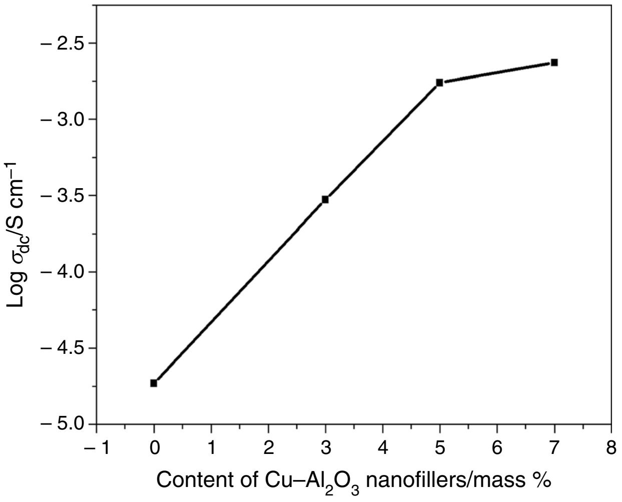

Fig. 14 DC conductivity of copolymer with different contents of Cu–Al_2O_3

Scarisbrick model

The theoretical Scarisbrick model evaluates the contribution of an ohmic inter-particle contact in generating a conductive network within the hybrid copolymer nanocomposites. According to this model, the conductivity of the conducting copolymer nanocomposites can be represented as

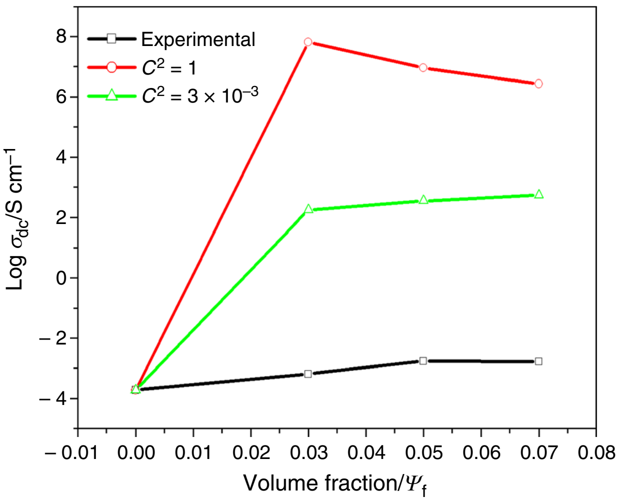

Fig. 15 Variation of DC conductivity with Scarisbrick model

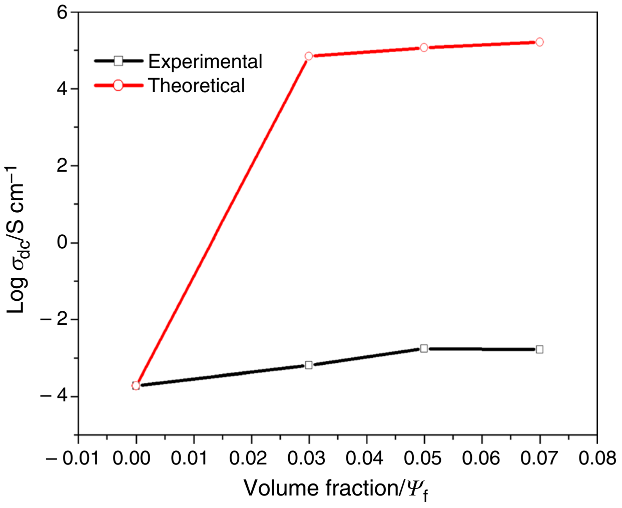

Fig. 16 Variation of DC conductivity with Bueche model

$$\frac{\sigma_c}{\sigma_f} = C^2\psi\psi\left[\exp\left(\psi^{\frac{-2}{3}}\right)\right] \tag{4}$$

where σ_c, σ_f, ψ and C is the conductivity of composite, conductivity of nanofillers, volume fraction of nanofillers in the hybrid and geometrical factor, respectively. The values of the geometrical factor (C^2) are ranging between 3×10^{-3} and 1. The comparison of conductivity obtained from Scarisbrick model and experimental conductivity is presented in Fig. 15. The theoretically obtained conductivity is higher in magnitude than the experimentally obtained conductivity. This huge variation in conductivity calculated from Scarisbrick model can be attributed to the disregarded contribution of the copolymer matrix toward conductivity [35]. Moreover, the difficulty in finding the actual values of the geometrical factor (C^2) also contributes to the aforementioned variations.

Bueche model

The Bueche model suggests that conductivity in heterogeneous hybrid systems arises from the physicochemical interaction existing between the copolymeric abutment and conductive fillers. The accumulation of nanofillers within the copolymeric abutment may generate a conductive path within the polymeric abutment. Thus, Bueche model considers the contribution of both filler particles and polymer toward conductivity [36]. The Bueche equation can be represented as

$$\sigma_c = \sigma_f\Psi_f + \sigma_p\left[1 - \psi_f\right] \tag{5}$$

where σ_f, σ_p, and Ψ_f correspond to the conductivity of filler, the conductivity of polymer and volume fraction, respectively. The graph comparing the experimental and theoretical conductivity (Bueche model) is represented in Fig. 16. It is evident that the Bueche model fails to explain the conductivity of the (PANI-*co*-PPy)/Cu–Al_2O_3 nanocomposites system. The failure of Bueche model can be attributed to the variable conductivity of constituents in the copolymer nanocomposite system.

McCullough model

McCollough model suggests that the DC conductivity of inorganic/copolymer hybrid nanocomposites depends on the filler content and conductive pathway generated between the interfaces [37]. The conductivity of copolymer nanocomposites using this model can be expressed as

$$\sigma_c = \sigma_p\Psi_p + \sigma_f\Psi_f - \left[\frac{\left[\lambda\psi_p\Psi_f + (\sigma_f - \sigma_p)^2\right]}{\nu_f\sigma_f + \nu_p\sigma_p}\right] \tag{6}$$

σ_f, σ_p, Ψ_f, Ψ_p and λ in this equation pertain to the conductivity of filler, the conductivity of the copolymer, the volume fraction of nanofillers, the volume fraction of the polymer and structural factor, respectively. The magnitude of the structural factor varies between 0 and 1. Using the following equations, the ν_f and ν_p values can be determined.

$$\nu_f = (1 - \lambda) \cdot \psi_f + \psi_p \cdot \lambda \tag{7}$$

$$\nu_p = (1 - \lambda) \cdot \psi_p + \psi_f \cdot \lambda \tag{8}$$

The values between 0 and 1 are substituted, and the theoretical DC conductivity is calculated. The theoretical DC conductivity calculated by McCollough model and experimental values is compared in Fig. 17. The graph suggests that for the value of $\lambda = 1$, the experimental conductivity and

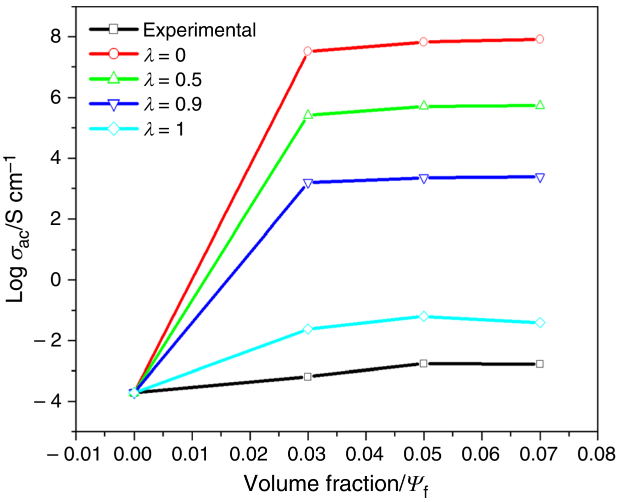

Fig. 17 Variation of DC conductivity with McCollough model

theoretical conductivity follow similar nature. The matching of experimental and measured conductivity values in this system indicates the formation of an excellent conductive network generated between the interface [38].

Conclusions

A series of conductive copolymer nanocomposites were prepared using poly(aniline-*co*-pyrrole) as a matrix and the conductive copper alumina as nanofillers. The bandgap energy obtained from the UV spectrum showed a decrease in optical bandgap energy of the composites with the addition of nanoparticles and the minimum bandgap energy observed for (PANI-*co*-PPy)/5 mass % Cu–Al_2O_3 nanocomposite indicated the presence of a large number of charge carriers in the hybrid system. The uniform dispersion of Cu–Al_2O_3 nanofillers in the copolymer was evident from FESEM images. The thermal stability of the copolymer nanocomposites obtained from TG analysis was significantly enhanced by the loading of Cu–Al_2O_3 nanoparticles. The AC conductivity, dielectric constant and dielectric loss parameters of all synthesized samples were found to increase with temperature and with the loading of nanofillers. The excellent AC electrical parameters observed for (PANI-*co*-PPy)/5 mass % Cu–Al_2O_3 nanocomposite are due to excellent electron tunneling between the interfaces. At higher loading of Cu–Al_2O_3 nanofillers, agglomerated filler particles in the copolymer block the conductive path and hence, electronic properties were significantly reduced. The Nyquist plot revealed the presence of bulk and grain boundary resistance in entire samples. In addition to this, this resistance was found to diminish with an increase in both the temperature and the content of nanofillers. The (PANI-*co*-PPy)/Cu–Al_2O_3 nanocomposites exhibited higher DC conductivity. The trend in DC conductivity with the content of nanofillers follows the McCullough theoretical model. The excellent electrical conductivity and dielectric properties of (PANI-*co*-PPy)/Cu–Al_2O_3 nanocomposites can be utilized for developing energy storage, optoelectronic and EMI shielding devices.

Declarations

Conflict of interest The authors of this article have no conflict of interest to declare.

References

1. Amorim DRB, Bellucci FS, Job AE, Guimarães IdS, da Cunha HN. Electrical, structural and thermal properties of new conductive blends (PANICG) based on polyaniline and cashew gum for organic electronic. J Therm Anal Calorim. 2019;136(4):1615–29. https://doi.org/10.1007/s10973-018-7778-6.
2. Sofiah AGN, Samykano M, Shahabuddin S, Kadirgama K, Pandey AK. An experimental study on characterization and properties of eco-friendly nanolubricant containing polyaniline (PANI) nanotubes blended in RBD palm olein oil. J Therm Anal Calorim. 2021;145(6):2967–81. https://doi.org/10.1007/s10973-020-09891-6.
3. Fisher C, Warmack BJ, Yu Y, Skolrood LN, Li K, Joshi PC, et al. All-aerosol-jet-printed highly sensitive and selective polyaniline-based ammonia sensors: a route toward low-cost, low-power gas detection. J Mater Sci. 2021;56(22):12596–606. https://doi.org/10.1007/s10853-021-06080-0.
4. Xu Y, Liu Q, You H, Zang L, Xiao Y, Wang X, et al. A facile patterning preparation of barnacle-like polypyrrole on sandpaper for flexible electronics. J Mater Sci. 2021;56(32):18162–73. https://doi.org/10.1007/s10853-021-06515-8.
5. Yamani K, Berenguer R, Benyoucef A, Morallón E. Preparation of polypyrrole (PPy)-derived polymer/ZrO_2 nanocomposites. J Therm Anal Calorim. 2019;135(4):2089–100. https://doi.org/10.1007/s10973-018-7347-z.
6. Zeng J-L, Sun S-L, Zhou L, Chen Y-H, Shu L, Yu L-P, et al. Preparation, morphology and thermal properties of microencapsulated palmitic acid phase change material with polyaniline shells. J Therm Anal Calorim. 2017;129(3):1583–92. https://doi.org/10.1007/s10973-017-6352-y.
7. Gheymasi AN, Rajabi Y, Zare EN. Nonlinear optical properties of poly(aniline-co-pyrrole)@ ZnO-based nanofluid. Opt Mater. 2020;102: 109835. https://doi.org/10.1016/j.optmat.2020.109835.
8. Khademi S, Pourabbas B, Foroutani K. Synthesis and characterization of poly(thiophene-co-pyrrole) conducting copolymer nanoparticles via chemical oxidative polymerization. Polym Bull. 2018;75(9):4291–309. https://doi.org/10.1007/s00289-017-2264-z.
9. Pattanayak P, Papiya F, Kumar V, Singh A, Kundu PP. Performance evaluation of poly(aniline-co-pyrrole) wrapped titanium dioxide nanocomposite as an air-cathode catalyst material for microbial fuel cell. Mater Sci Eng C. 2021;118:111492. https://doi.org/10.1016/j.msec.2020.111492.
10. Zare EN, Abdollahi T, Motahari A. Effect of functionalization of iron oxide nanoparticles on the physical properties of poly (aniline-co-pyrrole) based nanocomposites: experimental and

theoretical studies. Arab J Chem. 2020;13(1):2331–9. https://doi.org/10.1016/j.arabjc.2018.04.016.

11. Saini M, Shukla R. Silver nanoparticles-decorated $NiFe_2O_4$/polyaniline ternary nanocomposite for electromagnetic interference shielding. J Mater Sci Mater Electron. 2020;31(7):5152–64. https://doi.org/10.1007/s10854-020-03075-6.
12. Ascencio F, Bobadilla A, Escudero R. Study of NiO nanoparticles, structural and magnetic characteristics. Appl Phys A. 2019;125(4):279. https://doi.org/10.1007/s00339-019-2579-8.
13. Azizi A. Green synthesis of Fe_3O_4 nanoparticles and its application in preparation of Fe_3O_4/cellulose magnetic nanocomposite: a suitable proposal for drug delivery systems. J Inorg Organomet Polym Mater. 2020;30(9):3552–61. https://doi.org/10.1007/s10904-020-01500-1.
14. Suhailath K, Thomas M, Ramesan MT. Studies on mechanical properties, dielectric behavior and DC conductivity of neodymium oxide/poly (butyl methacrylate). Polym Polym Compos. 2021;29(8):1200–11. https://doi.org/10.1177/0967391120960658.
15. Wu Z, Qi J, Li F, Zhu X, Wang Z, Zhang G, et al. The coupling influence of UV illumination and strain on the surface potential distribution of a single ZnO micro/nano wire. Nano Res. 2016;9(9):2572–80. https://doi.org/10.1007/s12274-016-1143-5.
16. Zhu YF, Zhang L, Natsuki T, Fu YQ, Ni QQ. Synthesis of hollow poly(aniline-co-pyrrole)–Fe3O4 composite nanospheres and their microwave absorption behavior. Synth Met. 2012;162(3):337–43. https://doi.org/10.1016/j.synthmet.2011.12.015.
17. Ismail RA, Zaidan SA, Kadhim RM. Preparation and characterization of aluminum oxide nanoparticles by laser ablation in liquid as passivating and anti-reflection coating for silicon photodiodes. Appl Nanosci. 2017;7(7):477–87. https://doi.org/10.1007/s13204-017-0580-0.
18. Kakade MB, Ramanathan S, Kothiyal GP. Nano-alumina by gel combustion, its thermal characterization and slurry-based coating on stainless steel surface. J Therm Anal Calorim. 2013;112(1):133–40. https://doi.org/10.1007/s10973-012-2700-0.
19. Yahya SI, Rezaei A, Aghel B. Forecasting of water thermal conductivity enhancement by adding nano-sized alumina particles. J Therm Anal Calorim. 2021;145(4):1791–800. https://doi.org/10.1007/s10973-020-10452-0.
20. Lu D, Jiang J, Lu L, Liao X, Nesterov KM, Islamgaliev RK, et al. Hardness, electrical conductivity and thermal stability of externally oxidized Cu–Al_2O_3 composite processed by SPD. J Mater Eng Perform. 2017;26(5):2110–7. https://doi.org/10.1007/s11665-017-2660-4.
21. Menon SS, Thomas M, Ramesan MT. Synthesis, characterization, gas sensing, and electrical property evaluation of polyaniline/copper-alumina nanocomposites. Polym Compos. 2020;41(3):900–10. https://doi.org/10.1002/pc.25421.
22. Gürel EA, Toppare L, Hacaloglu J. Direct pyrolysis mass spectrometry to investigate the effects of dopants on characteristics of polypyrrole and its copolymers. J Therm Anal Calorim. 2013;111(2):1133–8. https://doi.org/10.1007/s10973-012-2495-z.
23. Zoromba MS, Hosny NM. Synthesis of Fe2O3, Co3O4 and NiO nanoparticles by thermal decomposition of doped polyaniline precursors. J Therm Anal Calorim. 2015;119(1):605–11. https://doi.org/10.1007/s10973-014-4170-z.
24. Sharma BK, Khare N, Sharma R, Dhawan SK, Vankar VD, Gupta HC. Dielectric behavior of polyaniline–CNTs composite in microwave region. Compos Sci Technol. 2009;69(11):1932–5. https://doi.org/10.1016/j.compscitech.2009.04.012.
25. Megha R, Ravikiran YT, Chethan B, Raj Prakash HG, Vijaya Kumari SC, Thomas S. Effect of mechanical mixing method of preparation of polyaniline-transition metal oxide composites on DC conductivity and humidity sensing response. J Mater Sci Mater Electron. 2018;29(9):7253–61. https://doi.org/10.1007/s10854-018-8714-z.
26. Amruth K, Abhimari KM, Sankar S, Ramesan MT. Synthesis, characterization, dielectric properties and gas sensing application of polythiophene/chitosan nanocomposites. Inorg Chem Commun. 2021;136(2): 109184. https://doi.org/10.1016/j.inoche.2021.109184.
27. Nihmath A, Ramesan MT. Fabrication, characterization, dielectric properties, thermal stability, flame retardancy and transport behavior of chlorinated nitrile rubber/hydroxyapatite nanocomposites. Polym Bull. 2021;78(11):6999–7018. https://doi.org/10.1007/s00289-020-03469-w.
28. Biryan F, Pihtili G, Demirelli K. Thermal studies and influence of the thermal decomposition on dielectric properties of a new coumarin copolymers. J Therm Anal Calorim. 2020;139(6):3871–85. https://doi.org/10.1007/s10973-019-08993-0.
29. Subburaj M, Ramesan MT, Pradyumnan PP. Preparation, characterization and conductivity studies of chlorinated natural rubber. AIP Conf Proced. 2014;1620:541–8. https://doi.org/10.1063/1.4898294.
30. Suhailath K, Ramesan MT. Effect of ceria nanoparticles on mechanical properties, thermal and dielectric properties of poly (butyl methacrylate) nanocomposites. Polym Compos. 2020;41:2344–54. https://doi.org/10.1002/pc.25542.
31. Gaur MS, Indolia AP, Rogachev AA, Rahachou AV. Influence of SiO_2 nanoparticles on morphological, thermal, and dielectric properties of PVDF. J Therm Anal Calorim. 2015;122(3):1403–16. https://doi.org/10.1007/s10973-015-4872-x.
32. Mannu P, Palanisamy M, Bangaru G, Ramakrishnan S, Kandasami A, Kumar P. Temperature-dependent AC conductivity and dielectric and impedance properties of ternary In–Te–Se nanocomposite thin films. Appl Phys A. 2019;125(7):458. https://doi.org/10.1007/s00339-019-2751-1.
33. Suhailath K, Ramesan MT. Investigations on the structural, mechanical, thermal, and electrical properties of Ce-doped TiO_2/poly(n-butyl methacrylate) nanocomposites. J Therm Anal Calorim. 2019;135(4):2159–69. https://doi.org/10.1007/s10973-018-7285-9.
34. Naz S, Durrani SK, Mehmood M, Nadeem M, Khan AA. Study of thermal, structural and impedance characteristics of nanocrystalline copper chromite synthesized via hydrothermal process. J Therm Anal Calorim. 2016;126(2):381–9. https://doi.org/10.1007/s10973-016-5520-9.
35. Scarisbrick RM. Electrically conducting mixtures. J Phys D Appl Phys. 1973;6(17):2098. https://doi.org/10.1088/0022-3727/6/17/316.
36. Bueche F. Electrical resistivity of conducting particles in an insulating matrix. J Appl Phys. 1972;43:4837–8. https://doi.org/10.1063/1.1661034.
37. McCullough RL. Generalized combining rules for predicting transport properties of composite materials. Compos Sci Technol. 1985;22:3–21. https://doi.org/10.1016/0266-3538(85)90087-9.
38. Suhailath K, Ramesan MT. Theoretical and experimental studies on DC conductivity and temperature dependent AC conductivity of poly (butyl methacrylate)/Nd doped TiO_2 nanocomposites. J Thermoplast Compos Mater. 2020;33(8):1061–77. https://doi.org/10.1177/0892705718817350.